technologies

MDPI

Article

Industrial Internet of Things (IIoT)-Based Monitoring of Frictional, Vibration, and Sound Generation in Lubricated Automotive Chains

Shubrajit Bhaumik [1,*], Krishnamoorthy Venkatsubramanian [2], Sharvani Varadharajan [2], Suruthi Meenachinathan [2], Shail Mavani [3], Vitalie Florea [4] and Viorel Paleu [5,*]

1 Tribology and Interactive Surfaces Research Laboratory (TRISUL), Department of Mechanical Engineering, Amrita School of Engineering, Amrita Vishwa Vidyapeetham, Chennai 601103, India
2 Department of Electronics and Communications Engineering, Amrita School of Engineering, Amrita Vishwa Vidyapeetham, Chennai 601103, India; k_venkatasubramanian@ch.amrita.edu (K.V.); sharvanivaradharajan@gmail.com (S.V.); suruthi1425@gmail.com (S.M.)
3 Mosil Lubricants Private Limited, 166/1, "KALANIDHI", Sion (West), Mumbai 400022, India; smavani@mosil.com
4 Department of Structural Mechanics, "Gheorghe Asachi" Technical University of Iași, 1 Prof. Dimitrie Mangeron Blvd, 700050 Iasi, Romania; vitalie.florea@academic.tuiasi.ro
5 Mechanical Engineering, Mechatronics and Robotics Department, "Gheorghe Asachi" Technical University of Iași, 43 Prof. Dimitrie Mangeron Blvd, 700050 Iasi, Romania
* Correspondence: s_bhaumik@ch.amrita.edu (S.B.); viorel.paleu@academic.tuiasi.ro (V.P.)

Abstract

This work assesses the frictional wear of lubricated transmission chains, correlating the coefficient of friction, root mean square (RMS) acoustic emissions, and vibrations induced by friction, incorporating Industrial Internet of Things (IIoT) components. The work is divided into two phases: understanding the frictional interactions between the steel pins of commercial transmission chain and high chrome steel plate (mimicking the interaction between the pin and roller of the chain) using a reciprocating tribometer (20 N, 2.5 Hz, 15.1 stroke length) in the presence of three commercial lubricant aerosols (Grade A, Grade B, and Grade C) and analyzing the frictional wear, sound, and vibration signals generated during the tribo-tests. In the second phase, the findings from the laboratory scale are validated using a commercial transmission chain under aerosol lubrication. Results indicated that the coefficient of friction in the case of dry conditions was 41% higher than that of Grade A aerosol and Grade C aerosol and 28% higher than that of Grade B aerosol. However, the average wear scar diameter on the pin with Grade C (0.401 ± 0.129 mm) was higher than that on the pins with Grades A (0.209 ± 0.159 mm) and B (0.204 ± 0.165 mm). Grade A and Grade B aerosols exhibited similar frictional conditions, while the wear-scar diameter in Grade C was the highest among Grades A and B but still less than in dry conditions. Analyzing the sound and vibrations generated during the friction test, it can be seen that the dry condition produced approximately 60% more sound level than the Grade A and Grade B conditions, and 41% more sound than the Grade C condition. The laboratory results were validated with a real-time transmission chain using an in-house chain wear test rig. Results from the chain wear test rig indicated that the elongation of the chain with Grade B is the least amongst the aerosols and dry conditions. The surface characterizations of the steel pins also indicated intense deep grooves and surface damage in dry conditions, with Grade A exhibiting the most severe damage, followed by Grade C, and the least severe in Grade B. Additionally, dark patches were visually observed on the rollers of the lubricated commercial chains, indicating stressed areas on the rollers, while polished wear was observed on the rollers under dry conditions.

check for updates

Academic Editor: Manoj Gupta

Received: 7 July 2025
Revised: 24 September 2025
Accepted: 29 September 2025
Published: 14 October 2025

Citation: Bhaumik, S.; Venkatsubramanian, K.; Varadharajan, S.; Meenachinathan, S.; Mavani, S.; Florea, V.; Paleu, V. Industrial Internet of Things (IIoT)-Based Monitoring of Frictional, Vibration, and Sound Generation in Lubricated Automotive Chains. *Technologies* **2025**, *13*, 465. https://doi.org/10.3390/technologies13100465

Copyright: © 2025 by the authors. Licensee MDPI, Basel, Switzerland. This article is an open access article distributed under the terms and conditions of the Creative Commons Attribution (CC BY) license (https://creativecommons.org/licenses/by/4.0/).

Keywords: sound; vibration-induced friction; transmission chains; industrial internet of things

1. Introduction

Engineering surfaces play a crucial role in the study of tribology [1], and a detailed analysis of the indirect feedback between interacting surfaces helps determine surface damage. Nowadays, utilizing concepts of "Tribotronics" by integrating various electronic components is gaining importance in larger systems and is an important part of the Industrial Internet of Things (IIoT). The Industrial Internet of Things enables the usage of various sensors to determine the health of industrial equipment [2] and is still regarded as an accurate approach in hard-to-reach areas, particularly between interacting surfaces. The acoustic emission (AE) technique effectively detects the damage on surfaces caused by friction [3]. The AE technique of non-destructive testing has been used for detecting friction and wear for a long time [4–6] under dynamic conditions; however, very limited work has been reported on correlating AE with frictional properties at the transition from static to dynamic conditions. Friction sounds are generated due to the deformations of the mating surfaces. Taura et al. [7] utilized AE and detected slip between the brass ball and the steel surface, reporting an increase in AE and frequency with increasing slip. Ferrer et al. [8] also discussed the use of AE in slip conditions between steel–steel interactions to determine the transition to dynamic friction, indicating that the AE technique can be used irrespective of the mating pair geometry. A system vibrates when it cannot dissipate the energy effectively. Vibrations also occur when friction is generated between two mating pairs, which reduces the efficiency of the equipment. Chen et al. [9] employed complex eigenvalue analysis (CEA) and transient dynamic analysis (TDA) to investigate vibrations under various conditions. Xu et al. [10] investigated the wear of steel-bearing surfaces using friction-induced vibration features and defined a feature parameter based on these features, thereby quantitatively characterizing the wear. Zhang et al. [11] studied the friction-induced vibration and noise generated in a graphene-reinforced high-density polyethylene (HDPE) and developed an HDPE composite with excellent anti-wear and vibration reduction properties. Furthermore, the surface morphology, contact pressure, and stick-slip also play a crucial role in controlling the vibration that occurs during friction.

Addallah et al. [12] also numerically and experimentally investigated the dynamic response of spur gears considering three different forms of friction-based vibration and concluded that a combination of friction-induced noise and the response from their numerical model can accurately simulate the dynamic behaviour of the gearbox. Hongling et al. [13] studied the vibrations induced due to the stick-slip in water bearings of a submarine. Additionally, they reported that the rotation speed, contact pressure, surface hardness, and lubrication conditions are responsible for the vibration induced by friction. Xue et al. [14] also noted the dependence of friction-induced vibrations on surface morphology and the presence of lubricants. Wang et al. [15] analyzed the influence of pit presence on taper roller bearings and reported a 45.1% reduction in friction and a 62.5% reduction in wear. Additionally, the presence of pits also reduced the vibrations and suppressed the acoustic emissions produced. As seen from the literature above, instantaneous RMS values of acoustic emissions have already been used to map friction and wear. In automotive applications, such as electric vehicles, it has become a crucial criterion to design chains with low acoustic emissions and minimal vibrations during operation.

Based on the preliminary observations, this study is built on two primary hypotheses. The first hypothesis proposes a measurable correlation between the coefficient of friction,

vibration, and acoustic emissions (RMS) in lubricated chains under frictional conditions, which can be effectively monitored using Industrial Internet of Things (IIoT) technologies. The second hypothesis explores the interdependence of friction, wear, and vibration as key indicators for assessing wear in transmission chains. Accordingly, the present work aims to investigate the correlation between acoustic emissions and the coefficient of friction generated between two steel surfaces in the presence of industrial-grade aerosol lubricants. Vibration induced during the friction process is also analyzed to establish a relationship between acoustic emissions, vibration, and the frictional coefficient recorded during laboratory-based tribological tests.

To the best of the authors' knowledge, no systematic study has been reported on using instantaneous RMS values of sound and vibration to predict failure or degradation of lubricated transmission chain components. To address this gap, this work seeks to validate the reliability of real-time RMS values as diagnostic indicators for chain wear and damage. Similarly, there are limited studies on the tribological performance of aerosol-lubricated chains, and no study has systematically correlated the coefficient of friction, wear, sound, and friction-induced vibrations under laboratory and real-time conditions. This research bridges these gaps by correlating these parameters through both laboratory-scale and component-level tests, conducted in two phases. In the first phase, frictional interactions between two steel surfaces (chain pin and high-chrome steel) are evaluated using a reciprocating tribo-test rig, with continuous recording and analysis of frictional forces, wear, sound, and vibration signals. In the second phase, findings from the lab-scale tests are validated using a commercial transmission chain mounted on a custom-built chain elongation test rig, under similar aerosol-lubricated conditions. Analysis of variance (ANOVA) is employed to evaluate significant differences among groups and the influence of lubricants [16]. A one-way ANOVA is used to compare the effects of lubrication conditions on sound level, vibration, coefficient of friction (CoF), and wear scar diameter (WSD). This comprehensive approach is expected to offer valuable insights for chain manufacturers, enabling predictive wear monitoring through real-time acoustic and vibrational analysis and promoting more efficient, condition-based maintenance strategies.

2. Materials and Methods

2.1. Materials

Steel pins from a commercially available transmission chain were dismantled from the chain to gain an in-depth understanding of the wear of the pins in transmission chains. These pins were used as mating pairs in the wear test. The counter body was a steel bar of EN 31. The composition of the pin and the steel bar was determined using an optical emission spectrometer (Make: Hitachi, Uedem, Germany, Model: OE 750) and is shown in Table 1.

Table 1. Chemical composition of pin and steel bar.

Tribo-Pair/ Elements	Element (%)							
	C	Mn	Si	S	P	Ni	Cr	Mo
Pin	0.406	0.568	0.186	0.012	0.010	1.345	1.115	0.221
Steel bar	0.943	0.334	0.195	0.011	0.008	-	1.505	-

The average surface roughness of the pins was measured to be 0.3501 ± 0.022 µm, and the roughness of the steel bar was maintained between 0.251 µm and 0.301 µm. The diameter of the pin was 2.5 mm, and the length was 20 mm. The pin hardness was found to be 63 ± 31.53 HRc, and the bar hardness was 25.6 ± 1.52 HRc. The hardness values are the

average of five hardness readings taken on the flat surface of the pin and the bar surface where both bodies would interact.

2.2. Measuring the Friction and Wear Using a Reciprocating Test Rig

The tribo-test used was a reciprocating test rig (Make: Magnum, Bengaluru, India) with a maximum loading capacity of 20 N and a speed of 2.5 Hz. A stroke length of 15.1 mm was maintained for all the tests. Three different commercial chain lubricant aerosols, Grade A, Grade B, and Grade C, were used during the test. The composition of the sprays was taken from the data available on the product data sheet (Table 2). Before the start of the experiment, a single layer of the lubricant was sprayed from the aerosol cans. Each test was repeated twice, and the average of the three readings has been reported here.

Table 2. Composition of the commercially available chain spray aerosol as available on the datasheet of the products.

Composition Type	Grade A	Grade B	Grade C
Carrier agent	A high molecular weight polymer (olefin + copolymer) doped with approximately 8% calcium sulphonate 400TBN.		
Anti-oxidant	Aminic anti-oxidant	Aminic anti-oxidants	Dothiocarbamate
Anti-wear additives	Phosphate ester	Nil	Nil

2.3. Industrial Internet of Things: Data Porting from the Real World to the Cloud

The experimentation setup (Figure 1) with ESP32 sorted the hardware constraints and the bulk update method, which serves up to 58 samples/minute, into the cloud platform. However, the proposed final setup does have complications in terms of the number of sensors that can be interfaced with the ESP32 controller. Only 6 analog sensors can be connected to the ESP32 controller at a time, as the ESP32 has two Analog-to-Digital-Channels (ADC) (ADC1 with 6 pins) and (ADC2 with 9 pins), but ADC channel 2 cannot be accessed when the Wi-Fi module is utilized. The ADC2 and Wi-Fi modules will use the same pins in different operating modes. Hence, 6 pins from ADC1 can only be used for sensors simultaneously with Wi-Fi under operation. The objectives can be further optimized with other controllers and subscribed versions of the cloud platform, which requires financial affordability. For this work, the available number of ADCs is sufficient.

Steps in Data Logging

Initialization: Setup includes defining variables and constants for sensor communication and ThingSpeak integration. This covers JSON buffers, WiFi credentials, GPIO pin assignments, and network management through WiFiClient. Timing variables track data transmission to the cloud.

Connecting to WiFi: The setup() function initiates serial communication and attempts WiFi connection in a loop. If unsuccessful, it waits 5 s before retrying. Upon a successful connection, it displays the network status, including the SSID and signal strength, to confirm reliable connectivity.

Uploading the data to the Cloud: The httpRequest function handles data transmission to ThingSpeak. It first closes any existing connections, then initiates a new server connection via the client connect(). Once connected, it sends an HTTP POST request containing our channel ID, along with the necessary headers (Host, User-Agent, and Content-Type: JSON), to ensure proper data routing to our ThingSpeak channel.

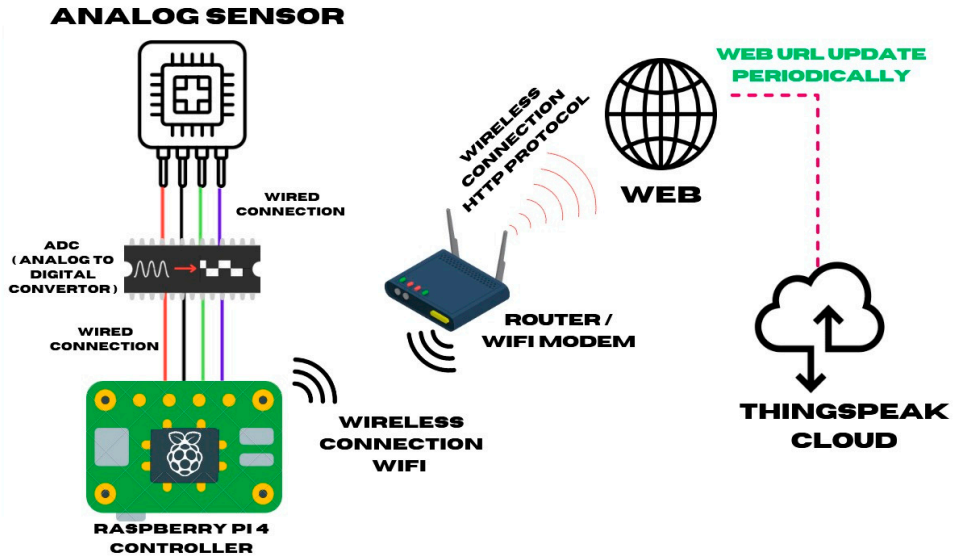


Figure 1. Schematic illustration of how the data is ported from the sensor world to the cloud space using ESP32 controller (IoT).

2.4. Measuring the Sound and Vibration Induced Due to Friction During the Tribo-Test Using Sensors Employing the Concept of Industrial Internet of Things

The sound and the vibration induced by friction during the wear test were recorded using acoustic sensors (two) and a vibration sensor. The acoustic sensors were placed on either side of the rubbing area, and the vibration sensor was attached to the pan on which the test specimen is mounted (Figure 2).

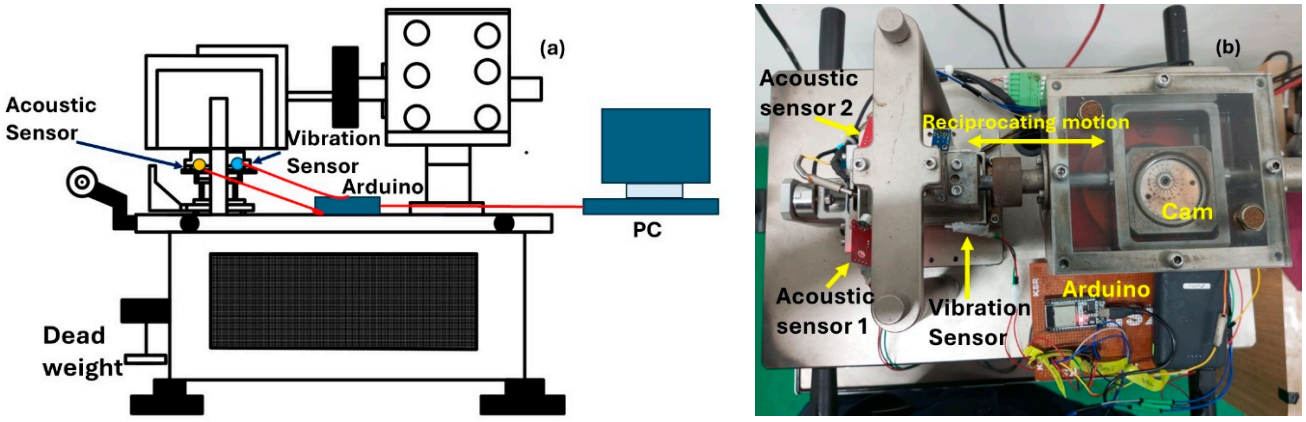


Figure 2. (**a**) Schematic diagram of the experimental set of reciprocating wear test rig (**b**) Sensors fitted to the test rig.

An acoustic sensor was employed to record the acoustic emission signals generated by friction and wear. This sensor features a sensitivity range of −60 to −56 dBV/Pa, operates at 5 V, and is capable of detecting converted acoustic signals within a 0 to 5 V range, digitally represented from 0 to 1023. The acoustic sensor includes a built-in audio amplifier using the LM386 chip from Texas Instruments, Dallas, TX, USA. The output from the microphone was linked to the audio amplifier circuit, as illustrated in Figure 3.

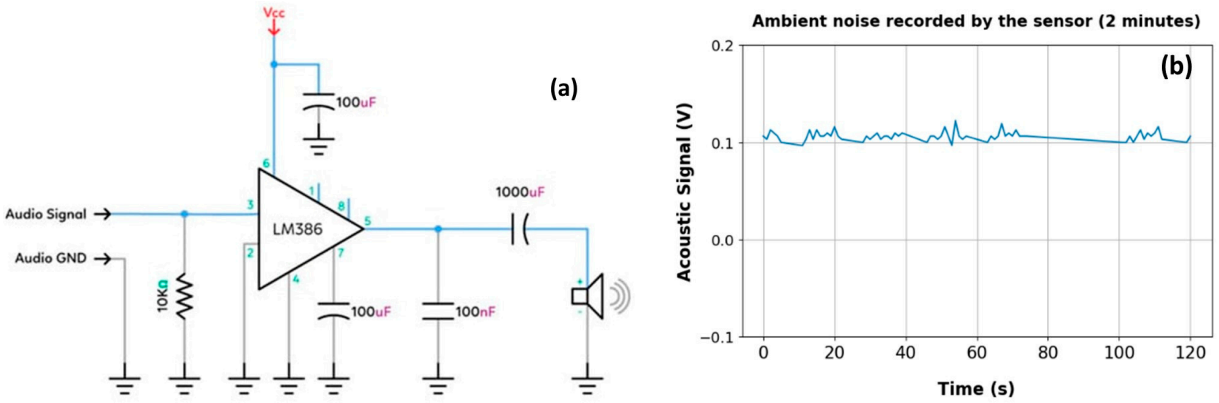


Figure 3. (**a**) LM386 audio amplifier circuit. (**b**) Ambient noise recorded by the acoustic sensor before the test.

In the amplifier circuit, pins 1 and 8 were left unconnected to maintain a default gain of 20, which was sufficient to capture the acoustic emissions produced by the contact between the two metals. Increasing the gain beyond this level resulted in excessive noise or amplified surrounding acoustic emissions. A 100 µF capacitor was placed between pin 7 and ground to eliminate any power supply noise from being amplified. In the circuit (refer to Figure 3), a 100 nF capacitor was utilized to filter out high-frequency noise, while a 1000 µF capacitor was employed to smooth out voltage ripples. The audio circuit was powered, and its output was directed to a spectrum analyzer. A variable input sinusoidal signal with frequencies ranging from 20 Hz to 20 kHz was applied, revealing a total harmonic distortion (THD) of 1.7%. This level of THD was considered acceptable for the intended application. The test involved connecting the acoustic sensor to an Arduino microcontroller using a built-in 10-bit analog-to-digital converter (ADC) and supplying it with a 5 V power source. The experiment lasted one hour, and the digital output of the ADC was transformed into an analog voltage using Equation (1).

$$V = D \cdot 3.3/1023, \quad (1)$$

where V is the analog value of the voltage, D is the digital value, 3.3 is the reference voltage provided to the ADC, and since it was a 10-bit ADC, the resolution of the ADC was $2^{10} = 1024$.

The data preprocessing involves reducing background noise, where the mean of the initial minute of data is subtracted from the entire 60 min of experimental data to capture the noise created by friction. Following this adjustment, the sensor values were standardized to match the scale of the coefficient of friction (ranging from 0 to 1) by dividing each sensor value by its maximum value. This standardization facilitated a comparison between the levels of the coefficient of friction and the acoustic sensor-mapped values, encompassing the maximum, minimum, and range of the coefficient of friction versus the maximum acoustic sensor value. Subsequently, a correlation was established between the coefficient of friction and the acoustic sensor's value to calibrate the sensor's output in terms of the coefficient of friction. The normalized sensor value is obtained using the formula in Equation (2):

$$N = S/M, \quad (2)$$

where N is the normalized sensor value, S is the sensor value, and M is the maximum sensor value.

Data was collected to capture the background noise, which included acoustic emissions from nearby electrical appliances, people walking nearby, and other miscellaneous noises near the testing setup. The data from the Arduino was transmitted to a PC using a USB port and read at a baud rate of 9600. To assess the error contributed by the background

noise, the ambient noise was recorded for 120 s. The post-processing of the acoustic signal ensured that the impact of the noise was minimized to a greater extent during the analysis of the frictional noise data. To record the vibration-induced friction during the test, a versatile LDT0-028K vibration sensor was used, which utilizes a 28 µm thick piezoelectric polyvinylidene fluoride (PVDF) polymer film with screen-printed silver ink electrodes. It was laminated onto a 0.125 mm polyester and attached to the specimen holding sample. The sensor's design effectively detects vibrations and mechanical stress, making it suitable for detecting friction-induced vibrations during the reciprocating test. The LDT0-028K sensor exhibits high sensitivity and flexibility, making it easy to integrate with microcontrollers such as the ESP-32. Its robust design allows it to withstand high impacts, and it operates effectively within a temperature range of 0 °C to 85 °C, with a storage temperature range of −40 °C to 85 °C. The sensor supports analog communication capabilities of up to approximately 70 VDC, with a sensitivity of 50 mV/g. The sensor's resonant frequency and sensitivity can be adjusted by modifying the mass or clamping length, enabling precise detection and measurement of vibrations tailored to specific applications. This adaptability enhances the sensor's utility across various fields, including structural health monitoring, automotive applications, and consumer.

Figure 4 illustrates the sensor calibrations. Figure 4a indicates the calibration curves across three independent runs for sound levels ranging from 0 dB to 5 dB. The sensor output varies linearly between 0 V and 1.6 V, with minimal run-to-run deviations. This demonstrates consistent sensor behavior and repeatability in mapping sound pressure levels to voltage. The vibration sensor calibration was refined by mapping the operating range of 0–2 m/s^2 acceleration to 0–1 V output. Figure 4b indicates the corrected repeatability plots across three independent calibration trials, compared to the ideal linear response. The results confirm that the LDT0-028K sensor exhibits high linearity, repeatability, and low trial-to-trial variation, making it reliable for capturing low-level vibrational responses in the tribological chain wear test rig. The spectrum of the combined acoustic signal (blue curve) reveals two distinct frequency regions: (i) ambient noise localized at low frequencies around 60 Hz (red band), and (ii) friction-induced acoustic emissions concentrated at higher frequencies around 600 Hz (green band) (Figure 4c). The separation of these components in the frequency domain demonstrates the IIoT-based sensing system's ability to distinguish between environmental noise and frictional signatures during chain operation. This analysis validates the reliability of the acoustic emission sensor in capturing friction-related phenomena while filtering out background noise effects.

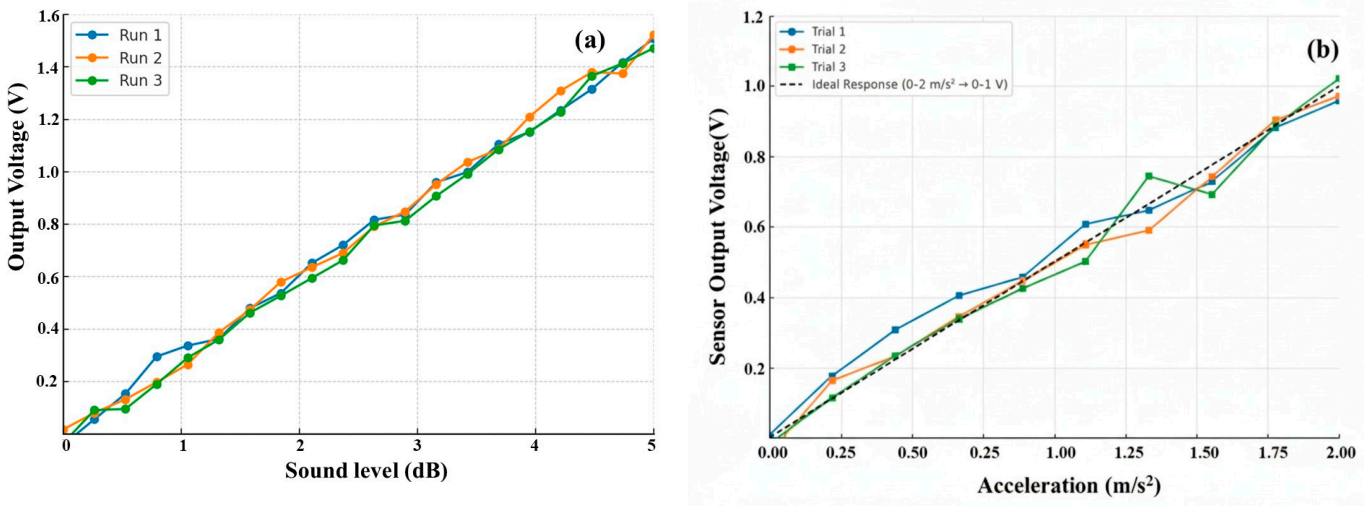


Figure 4. *Cont.*

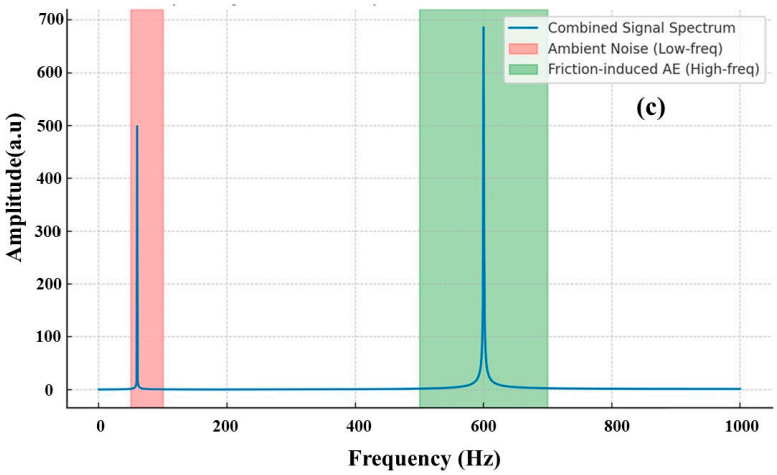


Figure 4. (**a**) Calibration and repeatability of acoustic sensor (**b**) Repeatability calibration of the vibration sensor (**c**) Domain Separation of Acoustic Emissions.

2.5. Validating the Tribo-Test Rig Results Using Commercial Transmission Chains

A customized chain wear test rig (Make: Magnum) was used to evaluate the wear resistance of commercially available transmission chains (Figure 5). The chain wear rig was subjected to an axial load of 1320 N, and the chain was rotated at 1500 rpm. The tests were run for 45 h. After every 15 h of running, the chain was inspected visually for surface damage and elongation. Eight different locations (bushes) were marked and selected to understand the wear patterns during the test. The tests were repeated twice. The objective of running this test was to validate the laboratory tribo test rig results in a real-time application.

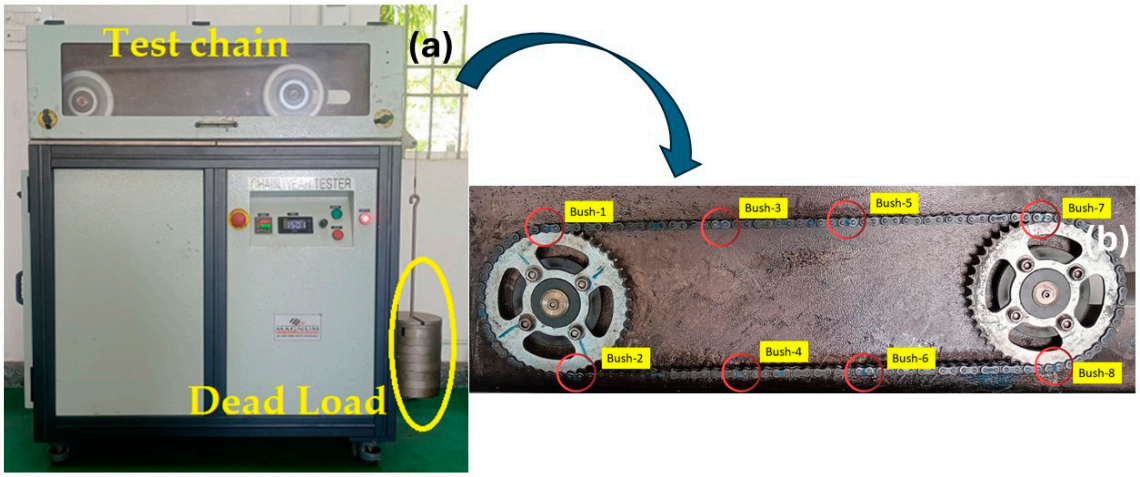


Figure 5. Customized chain wear test rig (**a**) full setup (**b**) test chain.

3. Results and Discussions

3.1. Investigating the Wear Properties of the Pin of a Transmission Chain Using a Reciprocating Wear Test Rig

Figure 6 indicates the average CoF and WSD during the tribology test. The coefficient of friction in the case of dry condition (0.5615 ± 0.037) was 41% higher than Grade A aerosol (0.0335 ± 0.0063) and Grade C aerosol (0.0355 ± 0.002) and 28% higher than Grade B aerosol (0.040 ± 0.0028).

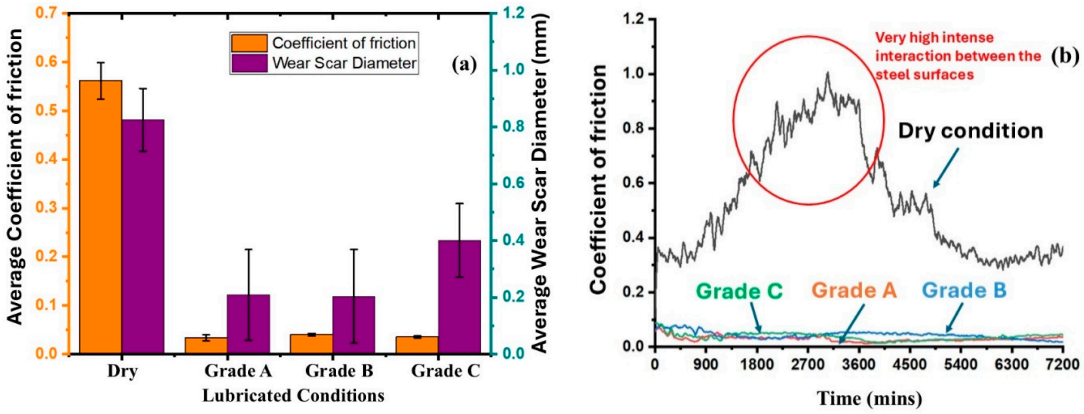


Figure 6. (**a**) Average coefficient of friction vs. average wear scar diameter on pin (**b**) Coefficient of friction vs. time.

The CoF in all the samples with aerosols exhibited similar frictional coefficients. However, the average wear scar diameter on the pin with Grade C (0.401 ± 0.129 mm) was higher than the pins with Grade A (0.209 ± 0.159 mm) and Grade B (0.204 ± 0.165 mm) (Figure 6a). The intense interaction between the mating pair in dry conditions can be identified with the high peak in the coefficient of friction graph (Figure 6b), which resulted in a high wear scar and a higher CoF. From Figure 7, it can be seen that the average sound and vibrations produced during the friction test in dry conditions were higher than the sound produced during the friction test using Grade A, Grade B, and Grade C aerosols; however, each of the aerosol lubricants behaved in different from each other, indicating that the composition of any lubricant would play a major role in controlling the acoustic emissions generation and vibration produced due to friction between the mating pair.

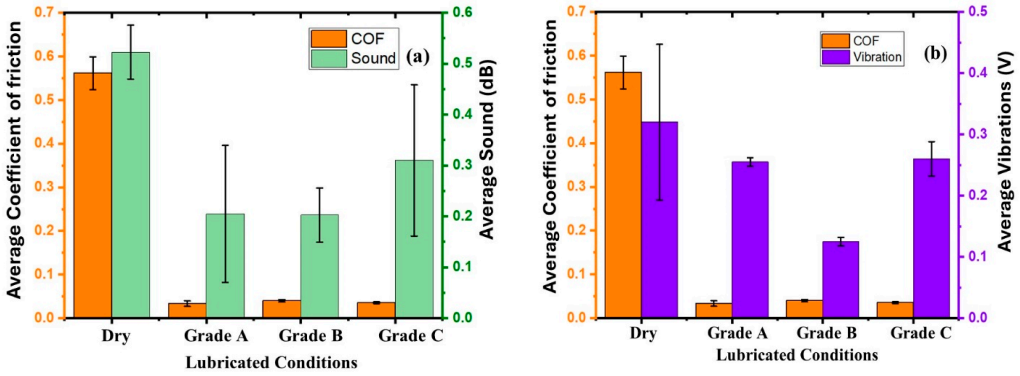


Figure 7. Average coefficient of friction: (**a**) average coefficient of friction with average acoustic emissions produced during the friction test, and (**b**) average coefficient of friction with average vibration produced during the friction test.

The test in dry conditions produced an average sound level of 0.522 ± 0.053 dB, while 0.205 ± 0.134 dB, 0.205 ± 0.053 dB, and 0.310 ± 0.148 dB were produced during the friction test with Grade A, Grade B, and Grade C aerosols (Figure 7a). Thus, the dry condition produced about 60% more sound emissions than Grade A and Grade B conditions and 41% more sound emissions than Grade C. Similarly, the dry condition (0.32 ± 0.127 V) produced 12% higher vibration than Grade A (0.255 ± 0.007 V) and Grade C (0.260 ± 0.028 V). The vibrations produced in the friction test using Grade B (0.125 ± 0.007 V) exhibited significantly lower vibration of 61% than in dry conditions and 51% lower vibrations than in Grade A and Grade C aerosols (Figure 7b).

Figure 8 exhibits the relationship between the average wear scar diameters, sound emissions, and vibrations produced during the tribo-test on the pins. It can be seen that the sound and the vibrations produced during the friction process correlated with each other (Figure 8a). High-wear scars produce more sound (noise) and vibrations, thus indicating an aggressive wear condition (Figure 8b). The average wear scar diameter in dry conditions (0.825 ± 0.11 V) was higher than in other lubricated conditions, so the sound produced was also higher in dry conditions. It is to be noted that the wear scar diameters in the case of Grade A (0.209 ± 0.159 V) and Grade B (0.204 ± 0.165 V) are equal, and hence, the sound produced during the friction was also similar. The vibrations recorded in the case of Grade B (0.125 ± 0.007 V) were the least among all the samples. It is interesting to note that even when the wear scars and acoustic emissions with Grade A and Grade B are almost equal, the vibrations produced in Grade A were higher than in Grade B. The increase in vibrations in Grade A as compared to Grade B may be due to the intense interaction between the mating pairs, which is confirmed by the increase in the roughness of the pin surface (Figure 8c). The percentage increase in roughness for Grade A (6.75%) and Grade C (5.32%) pins after the tests was greater than that for Grade B (3.21%).

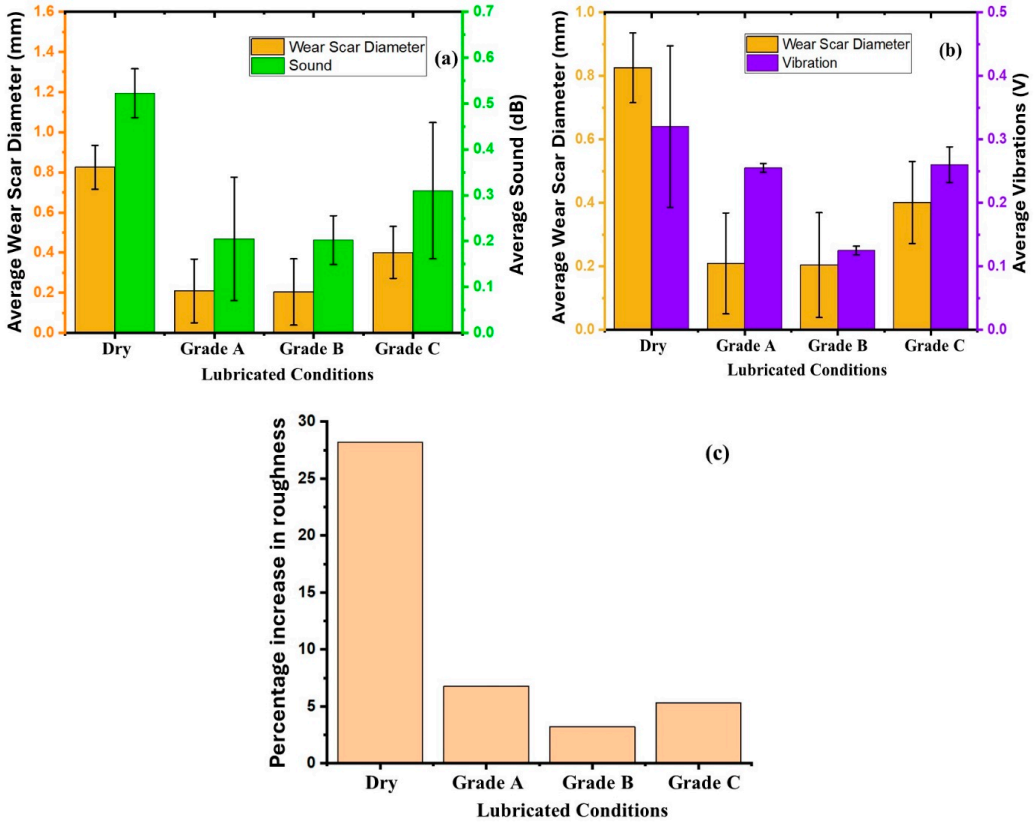


Figure 8. Percentage increase in roughness: (**a**) average wear scar diameter with average acoustic emissions produced during friction test, (**b**) average wear scar diameter with average vibration produced during friction test, and (**c**) percentage increase in average roughness of pins after tribo-test.

Figure 9 shows the optical microscope images of the wear scars of tribo-pairs. As shown in Figure 9a, the dry surface exhibited high wear, characterized by intense wear tracks, compared to the lubricated conditions. It is worth noting that the plate experienced more damage in all cases, with the highest damage occurring in dry conditions. In aerosol-sprayed conditions, surface damage is higher for Grades A and C compared to Grade B. Therefore, due to the surface damage in Grades A and C, the vibration levels were also higher in Grades A and C than in Grade B. The percentage increase in surface roughness seen earlier of the pins is also an indication of the intense metal-to-metal contact, the highest being in dry condition and

the least being exhibited by the pin of Grade B. From the results obtained in this work, it can be seen that even when friction and acoustic emissions follow a similar trend, the vibration induced due to friction may not follow a similar trend. Similar results correlating surface damage and friction-induced vibrations have also been reported by Qian et al. [17]. Thus, a non-interdependent nature between the frictional coefficient and sound generated during friction, along with the friction-induced vibration, can be established.

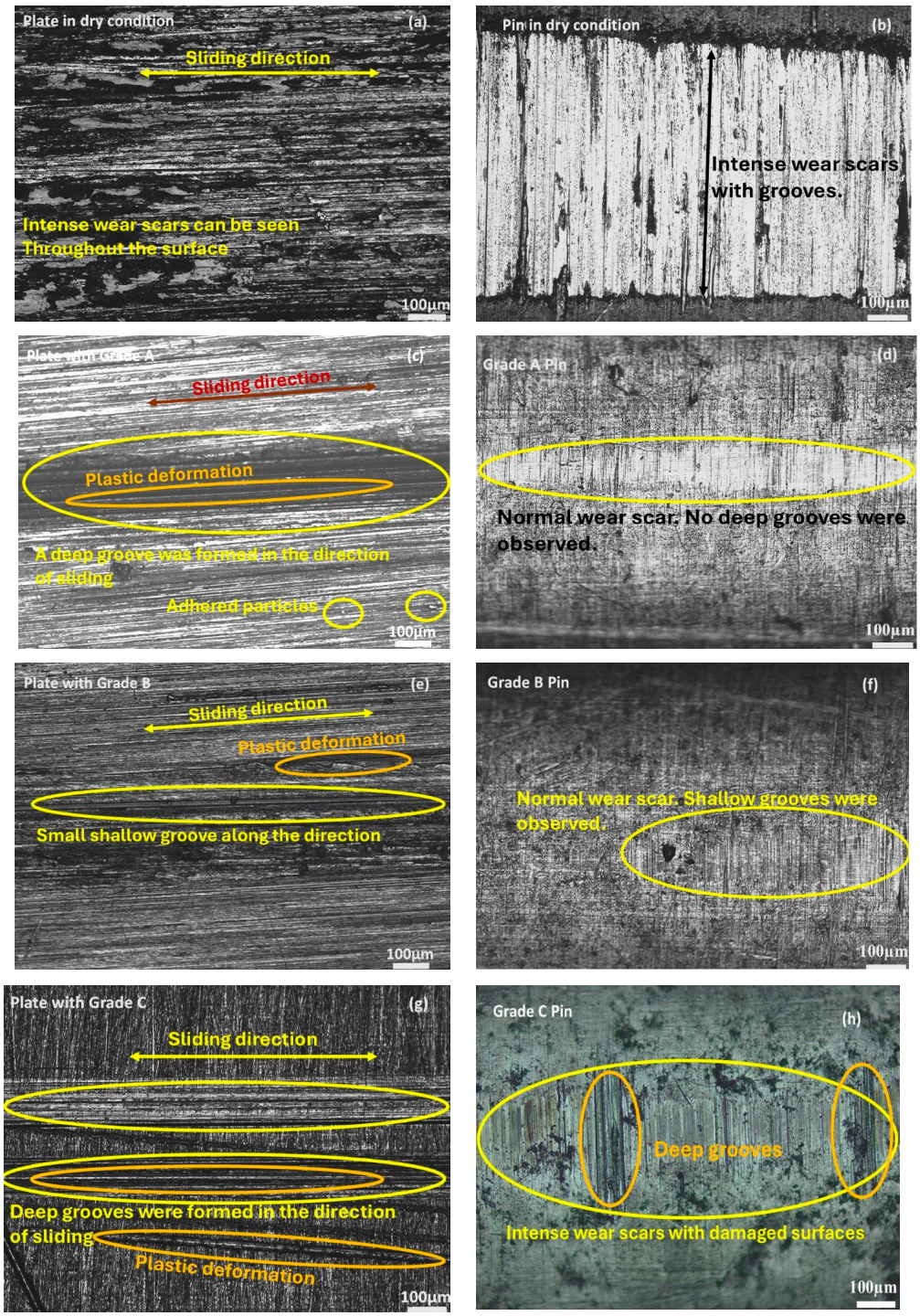


Figure 9. Optical microscopic images exhibiting the surfaces of (**a**) plate in dry condition, (**b**) pin in dry condition, (**c**) plate with Grade A, (**d**) pin with Grade A, (**e**) plate with Grade B, (**f**) pin with Grade B, (**g**) plate with Grade C, and (**h**) pin with Grade C.

3.2. Statistical Analysis of the CoF, WSD, Sound Generated, and Vibrations Using ANOVA

One-way ANOVA was used to analyze the outputs generated during the tests [18,19]. The one-way ANOVA showed significant group effects on CoF (p = 0.00000246) and WSD (p = 0.02967), whereas no effect was found for sound (p = 0.1088) and vibration (p = 0.15005) (Table 3). This shows that the experimental conditions had a greater impact on frictional and wear characteristics than on dynamic noise and vibration responses.

Table 3. ANOVA p-values.

Parameters	Sound	Vibration	COF	WSD
ANOVA p-values	0.11	0.15	0.00002	0.029

Pairwise t-tests indicated that there is a significant variation in CoF for dry test (DT) when compared to Grade A, Grade B and Grade C (DT-A, DT-B and DT-C), with significance from t-tests (Table 4). WSD indicated significant differences for the DT-A pair as well. By contrast, sound and vibration revealed few valid pairwise differences, with significance in DT-B (sound) and A-B (vibration).

Table 4. Pairwise t-test p-values.

Pair	p-Value			
	Sound	Vibration	COF	WSD
DT-A	0.14	0.48	0.023	0.042
DT-B	0.02	0.27	0.031	0.060
DT-C	0.26	0.62	0.031	0.074
AB	0.98	0.0048	0.61	0.976
AC	0.53	0.31	1	0.28
BC	0.48	0.078	0.22	0.32

DT—dry test, A—Grade A, B—Grade B, C—Grade C.

Pairwise comparisons were further tested using the Holm–Bonferroni correction. The adjusted threshold values were found to be smaller than the corresponding pairwise t-test p-values (Table 5), indicating that none of the pairwise differences reached statistical significance after controlling for multiple comparisons.

Table 5. Post hoc Holm threshold values.

Sample Pairs	Holm Threshold			
	Sound	Vibration	CoF	WSD
DT-A	0.01	0.025	0.00837	0.0083
DT-B	0.0083	0.0125	0.01	0.01
DT-C	0.0125	0.05	0.0125	0.0125
AB	0.05	0.0083	0.025	0.05
AC	0.025	0.0167	0.05	0.0167
BC	0.0167	0.01	0.0167	0.025

DT—dry test, A—Grade A, B—Grade B, C—Grade C.

Cohen's d values were evaluated and analyzed to find effect size (0.2 for small, 0.5 for medium, and 0.8 for large effects) (Table 6). Effect size analysis according to Cohen's d con-

firmed that the majority of pairwise comparisons between CoF and WSD were characterized by large effects, especially for the DT-A, DT-B, and DT-C pairs, affirming significant differences in friction and wear performance among these groups. Sound also revealed large effects for DT-A, DT-B, and DT-C, Vibration large effects for DT-A, DT-B and AB, and a medium effect for DT-C. As opposed to this, AC and BC pairs tended to have essentially zero effects on all parameters, indicating little difference between these two groups. The η^2 values showed variation of 95.6% for COF, 87.1% for WSD, 74.8% for sound, and 70.1% for vibration, although only CoF and WSD were statistically significant (Table 7).

Table 6. Cohen's d values for effect size.

Sample Pairs	Cohen's d Values			
	Sound	Vibration	COF	WSD
DT-A	3.10	1.05	19.27	4.92
DT-B	6.03	2.16	19.62	4.42
DT-C	1.90	0.65	19.81	3.52
AB	0.024	14.14	−0.66	0.033
AC	−0.74	−1.69	0	−1.43
BC	−0.96	−6.54	1.8	−1.32

DT—dry test, A—Grade A, B—Grade B, C—Grade C.

Table 7. ANOVA effect size η^2 values.

Parameters	Sound	Vibration	COF	WSD
ANOVA effect size η^2	74.8% of variability	70.1% of variability	99.6% of variability	87.1% of variability

The 95% confidence interval (CI) of Cohen's d, as approximated by the simple delta-method, added further information to the stability of these effect sizes. Significant differences were found at substantial intervals for DT-A (Sound, CoF, WSD), DT-B (Sound, CoF, WSD), and DT-C (CoF, WSD), supporting the existence of strong and stable differences. AB also revealed a significant difference for vibration, whereas BC revealed significance for CoF and vibration (Table 8). For most others, the CIs crossed with zero, suggesting no statistically reliable differences even though an effect size magnitude was observed.

Table 8. Approximate 95% CI for Cohen's d (simple delta-method approximation).

Sample Pairs	Cohen's d							
	Sound		Vibration		COF		WSD	
	CI d Lower	CI d Upper	CI d Lower	CI d Upper	CI d Lower	CI d Upper	CI d Lower	CI d Upper
DT−A	0.19	6.02	−1.03	3.14	5.77	32.77	0.98	8.85
DT−B	1.41	10.65	−0.30	4.63	5.88	33.36	0.78	8.05
DT−C	−0.45	4.26	−1.36	2.66	5.94	33.68	0.39	6.65
AB	−1.93	1.98	4.14	24.13	−2.67	1.35	−1.92	1.99
AC	−2.76	1.28	−3.98	0.58	−1.96	1.96	−3.62	0.76
BC	−3.03	1.10	−11.49	−1.60	−0.52	4.12	−3.49	0.83

DT—dry test, A—Grade A, B—Grade B, C—Grade C.

From above, it can be seen that DT-A and DT-B differences uniformly show strong, statistically significant effects on a variety of performance measures, specifically CoF and

WSD. The results confirm the previous ANOVA results by demonstrating that friction and wear measurements not only significantly vary between groups but also exhibit practically significant changes with large effect sizes. Conversely, comparisons between AC and BC are marked by insignificant effects, implying a larger similarity between the two groups.

3.3. Mapping Sound Generated and CoF During the Reciprocating Wear Test

The acoustic emissions were mapped with the CoF for each test as shown in Figure 10:

- Dry condition

Test 1: Initially, from 0 to 30 min, both acoustic emission signals and CoF remain relatively stable. As CoF starts to increase around the 30 min mark, both acoustic emission signals show slight increases in amplitude and variability, but not to the same extent as CoF. During the peak CoF period (40–60 min), Sound1 and Sound2 exhibit more fluctuations, but their overall amplitude does not match the dramatic rise in CoF. This suggests that while the sound generated responds to changes in friction, the relationship is not strictly linear. After 60 min, as the CoF decreases, both sound signals become more stable but exhibit greater variability than at the beginning of the test. The dry test conditions likely caused a significant increase in CoF, possibly due to higher adhesion or material transfer between the surfaces.

Test 2: Initially, from 0 to 30 min, all three parameters (Sound1, Sound2, and CoF) exhibit relatively stable behavior, with Sound2 displaying a slightly higher amplitude than Sound1. As the CoF begins to rise around the 30 min mark, an increased variability in both sound signals was observed, though their overall amplitude changes are less dramatic than the CoF increase. During the period of highest CoF (50–80 min), Sound1 and Sound2 exhibited correlation with the friction trends, displaying increased fluctuations. However, the magnitude of these acoustic changes is not proportional to the extreme CoF spike, suggesting a non-linear relationship between friction and acoustic emissions. After the 90 min mark, as CoF returns to its initial levels, both sound signals also stabilize but maintain a slightly higher variability compared to the test's start.

- Grade A:

Test 1: The graph illustrates the interaction between Sound1, Sound2, and CoF during a Grade A test on a reciprocating test rig over 120 min. Sound1 remains stable around 0.2 dB, indicating consistent operation throughout the test. However, Sound2 shows noticeable fluctuations, particularly between 20:00 and 60:00 min, where its amplitude increases from 0.4 dB to above 0.5 dB, suggesting an increase in mechanical vibrations or surface interactions. Between 60 and 100 min, the system maintains lower friction and acoustic emission levels, indicating a period of smooth operation. However, at 100 min, there is a sharp increase in Sound2 followed by a gradual rise in CoF, signaling a breakdown of the beneficial conditions—possibly due to lubricant depletion or a shift in wear mechanisms.

Test 2: The graph shows the relationship between Sound1, Sound2, and the CoF. Initially, from 0 to 20 min, Sound2 closely follows the fluctuations in CoF, indicating a strong correlation. In contrast, Sound1 displays less pronounced peaks, suggesting it might be less sensitive to the friction changes observed in this period. During this time, the CoF stabilizes around 0.06 with minimal fluctuations. Sound2 remains relatively constant around 0.14 dB, consistently higher than Sound1, which averages around 0.08 dB. This implies that Sound2 may be more attuned to the overall friction conditions, while Sound1 might be detecting subtler surface interactions. The notable increase in both Sound1 and Sound2 at the 40 min mark, coinciding with a brief rise in the CoF, suggests that this rise in acoustic emissions levels could imply the surface is experiencing more significant wear, resulting in greater sound generation. In the final phase (80–120 min), an interesting inverse

relationship emerges: as the CoF gradually decreases from 0.06 to 0.02, the amplitude and variability of Sound1 increase significantly, eventually approaching the levels of Sound2. This shift indicates a change in wear mechanisms or surface conditions.

- Grade B:

Test 1: From 0 to 20 min, the CoF exhibits high-amplitude fluctuations, ranging from approximately 0.06 to 0.09. During this time, Sound1 shows significant variations, peaking around 0.4 dB before rapidly decreasing, suggesting that Sound1 is highly sensitive to the initial break-in period of the surfaces. At the 40 min mark, an anomaly occurs with a sharp spike in CoF, reaching approximately 0.08, yet neither Sound1 nor Sound2 displays a corresponding spike. This indicates a macroscopic friction event that did not significantly alter the sound emissions, possibly due to the presence of debris particles. Toward the end, the CoF stabilizes around 0.04 to 0.05, while both Sound1 and Sound2 remain constant. Sound2 consistently measures around 0.4 dB, notably higher than Sound1. The CoF then gradually decreases from approximately 0.04 to 0.02, suggesting a smoothing of the surface.

Test 2: The CoF fluctuates significantly in the initial phase, ranging from 0.07 to 0.08, with Sound2 exhibiting high-amplitude spikes of up to 0.9 dB, while Sound1 stabilizes at around 0.1 dB. During the transition phase, CoF stabilizes at 0.03–0.04, and both acoustic emissions exhibit low levels, indicating a decoupling of friction and acoustic signals. The major anomaly, occurring around 65 min, is characterized by a dramatic spike in Sound2 to 1.0 dB, accompanied by only a minor increase in CoF. This suggests that the event, possibly caused by a significant debris particle or sudden surface change, did not substantially affect the overall friction. In the final phase, the gradual decrease in CoF from 0.05 to 0.02, indicative of potential surface smoothing, does not impact acoustic emissions, which remain steady.

- Grade C:

Test 1: From 0 to 60 min, Sound1 and Sound2 exhibit relatively stable patterns, with Sound2 showing slightly higher amplitude. During this time, CoF fluctuates between 0.04 and 0.06, indicating some variability. At the 60 min mark, a significant change occurs. Sound1 jumps from 0.4 to 0.6 dB and stays there, while Sound2 drops sharply from 0.5 to 0.2 dB. This sudden change in acoustic emissions levels corresponds with a significant drop in CoF from 0.05 to 0.02, suggesting a decrease in friction. This gradual rise in CoF correlates with subtle increases in both Sound1 and Sound2, as the rise in CoF may indicate that while the system is returning to a higher friction state, the mechanical changes are also affecting the sound signals.

Test 2: In this graph comparing Sound1, Sound2, and the CoF for Grade C—Test 2, we observe distinct patterns and correlations over the 120 min test period. Initially, from 0 to 40 min, there is significant variability in the CoF, fluctuating between 0.04 and 0.06, while Sound1 and Sound2 remain relatively stable, with Sound2 consistently higher than Sound1. Around the 40 min mark, there is a noticeable shift: the CoF starts to decline steadily, reaching its lowest point of around 0.02 at 60 min. After this, the CoF gradually rises again, ending at about 0.04 by the end of the test. Throughout this period, both Sound1 and Sound2 stay relatively stable, with Sound2 still higher. However, there is a sharp spike in CoF just after the 100 min mark that is not reflected in either acoustic emissions measurement.

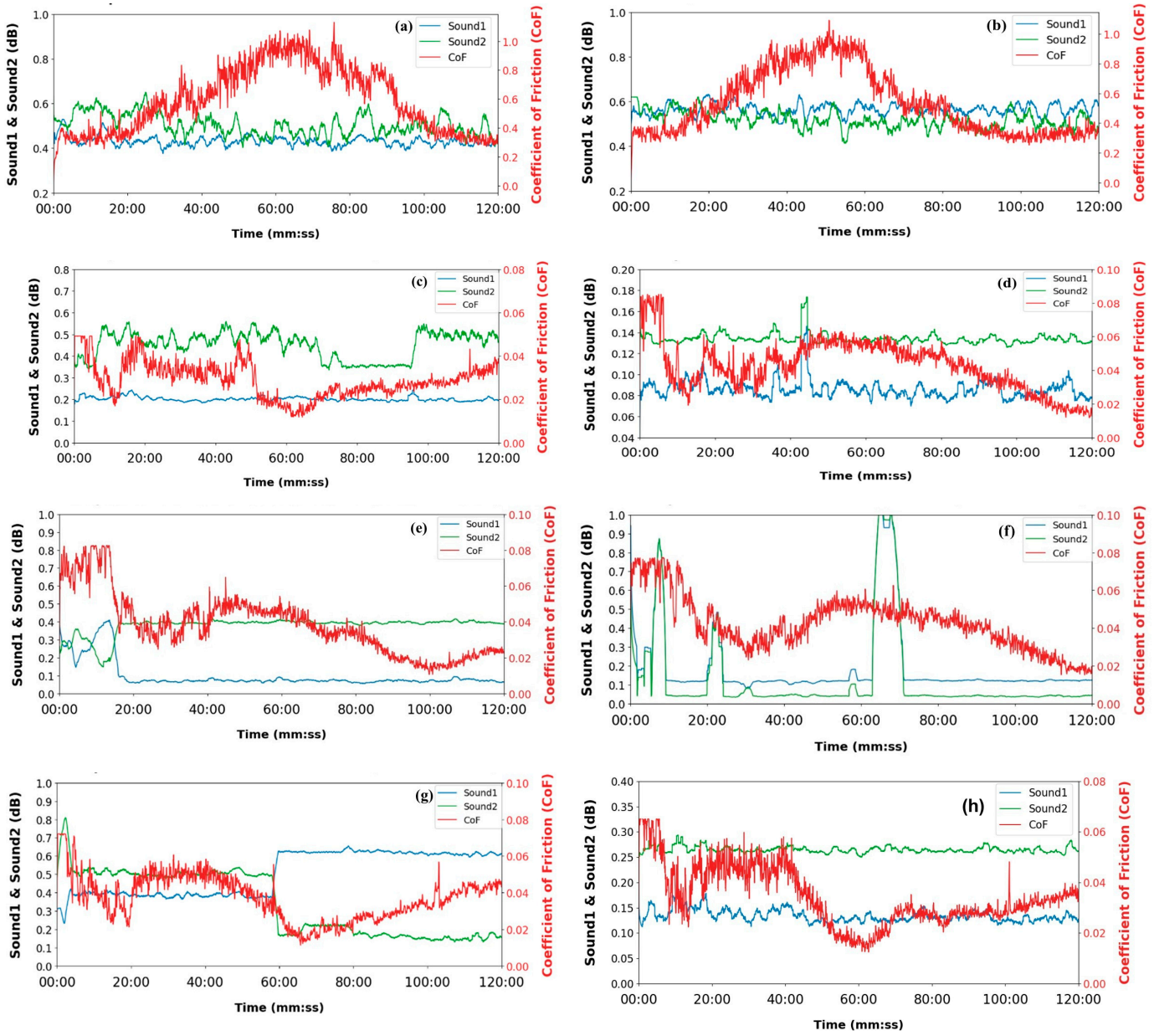


Figure 10. Mapping the sound generated and coefficient of friction during wear test: (**a**,**b**) dry condition, (**c**,**d**) Grade A, (**e**,**f**) Grade B, and (**g**,**h**) Grade C.

3.4. Mapping Friction-Induced Vibrations and CoF During the Wear Test

The vibration produced during the friction test was mapped with the CoF recorded during the wear test (Figure 11). The following has been observed during the wear test:

- Dry condition:

Test 1: Initially, both start at relatively low values, indicating a stable state with minimal friction and vibration. Between 00:00 and 40:00 min, CoF rises significantly, peaking at around 60 min, while Vibration shows a slight increase and spikes at around 80 min. Towards the end, CoF stabilizes at a lower value, and vibration shows a slight increase at the very end.

Test 2: In the initial phase, the vibration level sharply increases, indicating the onset of surface interaction, which subsequently decreases as the system stabilizes. Simultaneously, the CoF starts low and gradually increases During the middle phase, both vibration and CoF remain stable, with periodic spikes. These fluctuations indicate moments of higher

resistance or micro-impacts on the surface. Towards the end, during 80 min both vibration and CoF decrease to a more stable state with coinciding trends.

- Grade A:

Test 1: The vibration and CoF exhibit varying correlations throughout the test. Both parameters decrease initially and then exhibit gradual fluctuations, with certain periods where the trends align closely, especially during the 20 min and 40 min intervals, where the peak in vibration coincides with the peaks in CoF. They follow a similar trend during the middle to later stages of the test (beyond 40 min). Towards the end of the test, both begin to show an upward trend, with some spikes corresponding to their increase, indicating the onset of wear that leads to an increase in friction.

Test 2: The CoF and vibration start with a high value and then gradually decrease, with vibration oscillations settling towards 0.3 V. The vibration exhibits a consistent pattern of rises and falls, with coinciding peaks between 20 and 40 min. CoF gradually decreases to lower values towards the end of the test, suggesting stabilization in friction characteristics. Vibration also exhibits a similar curve to that of CoF during the 80 to 100 min.

- Grade B:

Test 1: The CoF begins with a relatively high value and sharp fluctuations. There is an overlap in the pattern of both parameters during the initial phase from 20 to 40 min showing a consistent trend. Between 60 and 70 min, the vibration peak aligns with the trends in CoF, after which CoF gradually stabilizes and starts decreasing, with fewer fluctuations, indicating reduced frictional resistance.

Test 2: The vibration shows a consistent trend with the CoF throughout the test, with intervals where its peaks coincide. Both CoF and vibration start high, and there is a similar drop within the first 10 min. Between 30 and 50 min, there is a clear correlation where peaks of vibration coincide with a slight increase in the CoF, and a similar trend between 60 and 80 min with overlapping peaks and troughs, suggesting the changes in frictional resistance. CoF and vibration gradually decrease towards the end of the test.

- Grade C

Test 1: In the initial phase, there is a noticeable overlap between the vibration and CoF, both with a high amplitude and downward trend. They have a similar pattern between 20 and 60 min with coinciding peaks. After 60 min, both follow a similar increasing trend. In the final phase (from 90:00 to 120:00), both signals exhibit a general upward trend, with occasional spikes indicating wear of the contact surfaces.

Test 2: Initially, both start at relatively low values, indicating a stable state with minimal friction and vibration. Between 00:00 and 40:00 min, CoF rises significantly, peaking at around 60 min, while vibration shows a slight increase and spikes at around 80 min. Towards the end, CoF stabilizes at a lower value, and vibration shows a slight increase at the very end.

Summarizing the observations from Sections 3.3 and 3.4, it can be seen that although the CoF-sound generated and vibration-wear correlate well throughout the experiment, there are situations where the sound generated and vibrations sometimes spike independently. This spike in CoF and vibrations in a dynamic tribo system is due to the high wear that occurs at that instant, resulting from the instability of the lubricant film that leads to its rupture at that particular instant, thereby causing excessive wear. The occurrence of high wear has already been observed from the deep groove formation and damaged surfaces, as shown in Figure 9 [20].

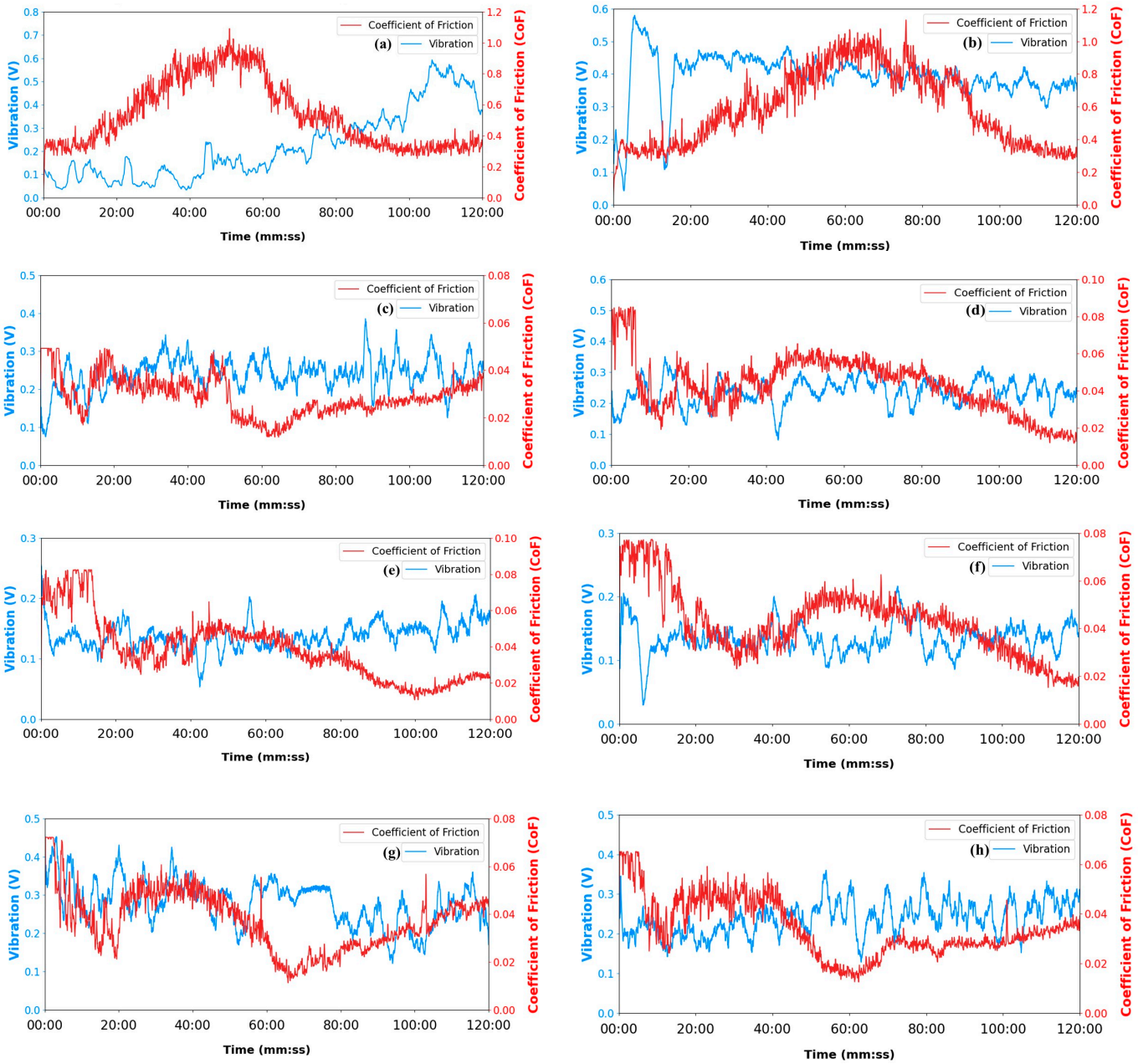


Figure 11. Mapping the vibration and coefficient of friction during wear test (**a**,**b**) dry condition (**c**,**d**) Grade A (**e**,**f**) Grade B (**g**,**h**) Grade C.

3.5. Tribo-Mechanisms Towards the Generation of Acoustic Emissions and Vibration Induced Due to Friction

The results from both dry and lubricated wear tests indicate that both acoustic emissions and vibration readings need to be considered when correlating them with tribological properties. A good correlation exists between surface damage and acoustic emissions produced. High friction and high wear will produce high acoustic emissions due to the increased dislocation densities caused by plastic deformations. The higher acoustic emissions, along with high vibration values, are a clear indication of extensive asperity interaction between the two bodies in dry conditions [21]. These acoustic emissions and the vibration values were reduced in the presence of aerosols, which created a lubricating film on the surface. Although the coefficient of friction between all the samples with aerosol was nearly identical, the acoustic emissions exhibited by Grade A and Grade B were similar to each other. In contrast, those of Grade C were higher compared to Grades A and B. This raised

an interesting point: whether the frictional coefficient and acoustic emissions should be investigated without further evaluation of other parameters, such as the vibration induced by friction. Geng et al. [22] reported a poor correlation between acoustic emission and load due to the suppression of friction-induced plastic deformation by the oxide layer fracture noise occurring in dry friction of steel. Hence, the vibration readings were investigated and were observed to follow a slightly different trend than the coefficient of friction in relation to the aerosol performance. Even though the acoustic emissions were similar for Grade A and Grade B, the vibration readings were lowest in the Grade B sample. Correlating the vibration readings with the coefficient of friction, it can be seen that the dry condition exhibited the highest vibrations, consistent with its highest coefficient of friction, even though the coefficients of friction in the samples were similar. Still, vibrations were least in Grade B and almost similar in Grades A and C.

High vibrations in dry, Grade A, and Grade C conditions are related to the extent of surface damage, such as intense deep grooves on wear scars, plastic deformations, and adhered particles. Zhang et al. [11] also reported that the formation of cracks on the surfaces of the mating pairs increases the vibration induced by friction. The present work exhibited higher surface damage in dry, Grade A, and Grade C conditions compared to Grade B. Consequently, the vibrations in the case of Grade B were the least, followed by Grade A and Grade C, with the highest being in dry conditions. Geng et al. [22] reported the formation of various iron oxides on the surface of the mating pair and their profound effects on the sound emissions. The oxide particles are crushed, and the noise from the oxide fracture is detected by the acoustic sensor. The vibrations caused during this crushing are also captured by the sensors during the vibration measurement. The Raman spectra of the wear scars on the pin and the plates indicated the formation of iron oxides (Figures 12 and 13). The Raman peaks at 300 cm^{-1} to 670 cm^{-1} are almost similar to those reported by De Faria et al. [23], indicating the formation of iron oxides. These oxide layers prevent direct contact between the mating pairs. It can be observed that the Raman peaks are more intense, with strong peaks of iron oxides, in dry conditions compared to the Raman peaks of aerosol-lubricated samples. This results in higher acoustic emissions and vibrations in dry conditions compared to the aerosol-lubricated samples.

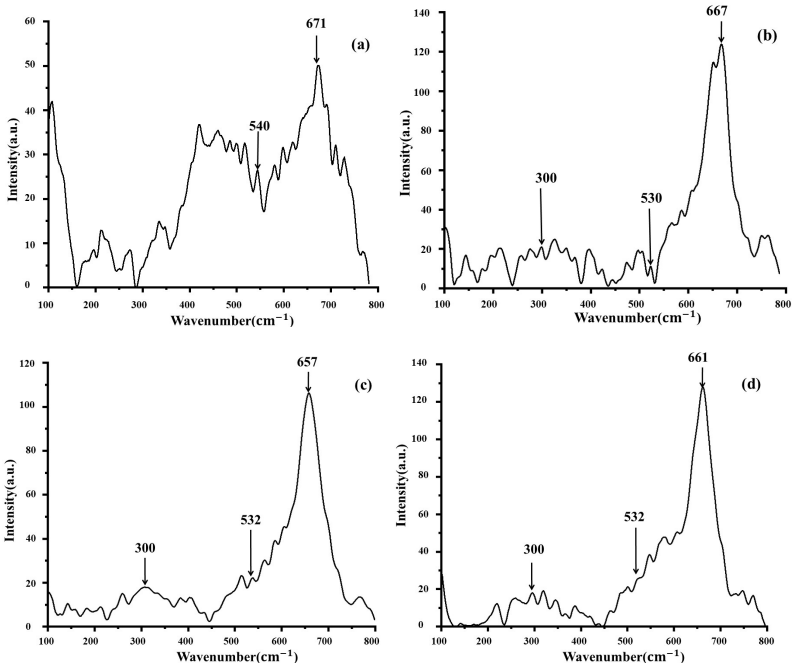


Figure 12. Raman Spectra of the wear scar on the pin after reciprocating test: (**a**) dry, (**b**) Grade A, (**c**) Grade B, and (**d**) Grade C.

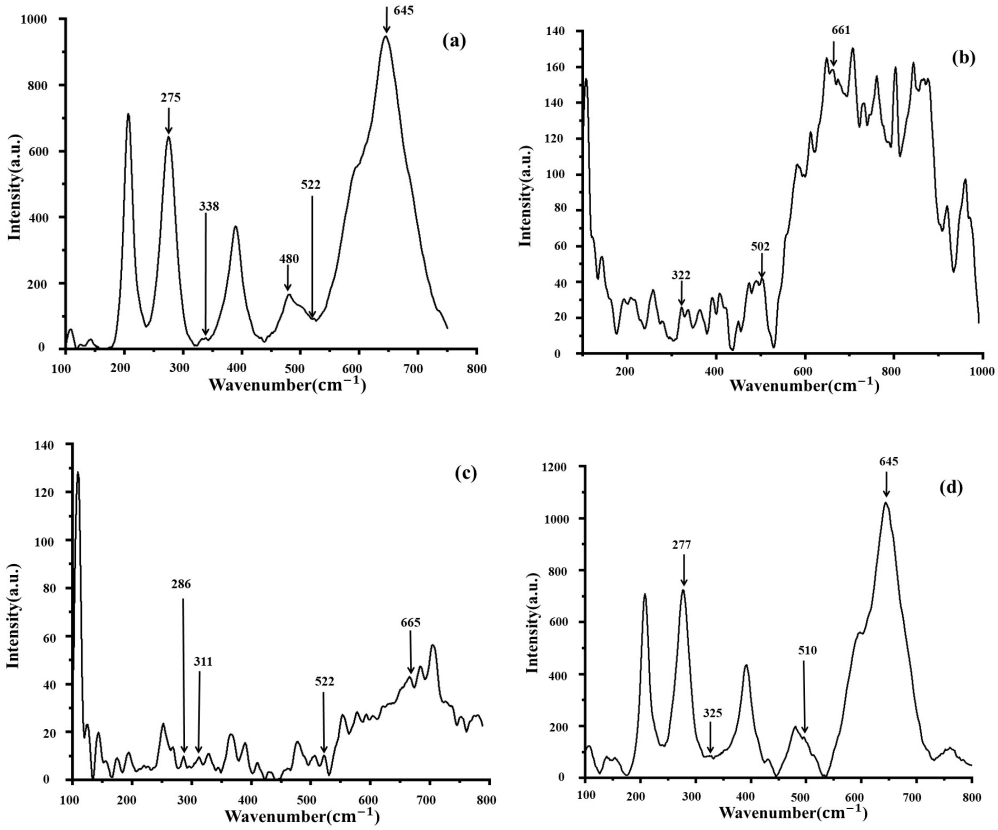


Figure 13. Raman Spectra of the wear scar on the plate after reciprocating test: (**a**) dry, (**b**) Grade A, (**c**) Grade B, and (**d**) Grade C.

3.6. Determining the Chain Wear Elongation Using the Chain Wear Test Rig and Correlating with the Results from the Reciprocating Rig (Component Level Testing)

The chain wear test rig was used to measure the chain elongation and the wear occurring in the chain. Figure 14 exhibits the percentage of chain elongation under dry and lubricated conditions. The percentage of chain elongation is significantly high under dry conditions. The chain elongation with Grade A was 51% (0.155 ± 0.059 mm) less than the elongation produced by the chain in dry condition (0.324 ± 0.071 mm) after 15 h. Additionally, with Grade A, the chain was 51% (0.229 ± 0.026 mm) and 61% (0.441 ± 0.058 mm) less elongated than the chain in dry condition after 30 h (0.447 ± 0.068 mm) and 45 h (0.622 ± 0.073 mm), respectively.

Grade B chain (0.124 ± 0.037 mm) exhibited 61% less chain elongation than the chain under dry conditions (0.324 ± 0.071 mm) and 20% less chain elongation than the Grade A sprayed chain (0.155 ± 0.059 mm) after 15 h. After 30 h, the chain sprayed with Grade B chain (0.22 ± 0.037 mm) exhibited 50% less elongation than the chain under dry conditions, while it exhibited only 4% less elongation than the chain with Grade A lubrication (0.229 ± 0.026 mm). Furthermore, after 45 h, the Grade B sprayed chain (0.293 ± 0.049 mm) exhibited 53% less elongation than the chain in its dry condition (0.622 ± 0.073 mm). Grade C sprayed chains (0.127 ± 0.032 mm) indicated about 61% less elongation (similar to the chain with Grade B aerosol) than the chain in dry condition after 15 h. Those chains also exhibited 50% less elongation after 30 h (0.234 ± 0.038 mm) and 45% less elongation after 45 h (0.339 ± 0.032 mm) as compared to the chain in dry condition. Considering these observations, it was further noted that the chains with Grade B exhibited the least elongations among all the chains, indicating the superior performance of Grade B lubricant than Grade A and Grade C. exhibited dark patches, indicating that the chains were stressed and, hence, more elongated than the chain with Grade B. Interestingly the vibration and the wear scar diameter exhibited by the reciprocating test matches are in line with the results from the

chain wear test. Thus, it emphasizes that the frictional coefficient and acoustic emissions may follow a similar trend, but the wear rate and vibration may not follow a similar trend to the frictional coefficient. Additionally, the vibration trend is more likely to follow the wear rate trend, as vibrations are generated due to misalignment. As the surfaces degrade, there is a high possibility that the system becomes misaligned, leading to higher vibration counts. Figure 15 shows the digital pictographs of the roller of the commercial chain, which was running under dry and aerosol-lubricated conditions. It can be seen that the chain in dry condition exhibited highly polished wear; thus, the elongation of the chain in dry condition was the highest. The chains with Grade A and Grade C exhibited more dark patches than the chain with Grade B, indicating stressed mechanical components in Grade A and Grade C than in the Grade B aerosol-sprayed chain. These component-level results align with the wear test results obtained using the reciprocating tribometer.

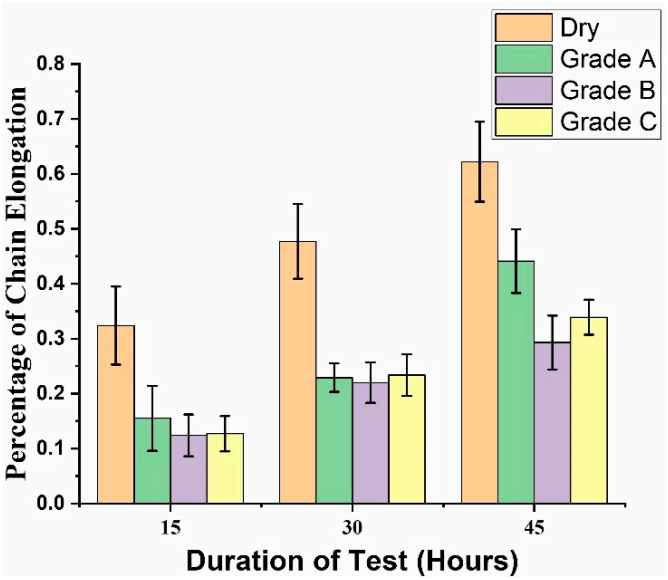


Figure 14. Percentage of elongation of chains under different types of aerosol lubrication.

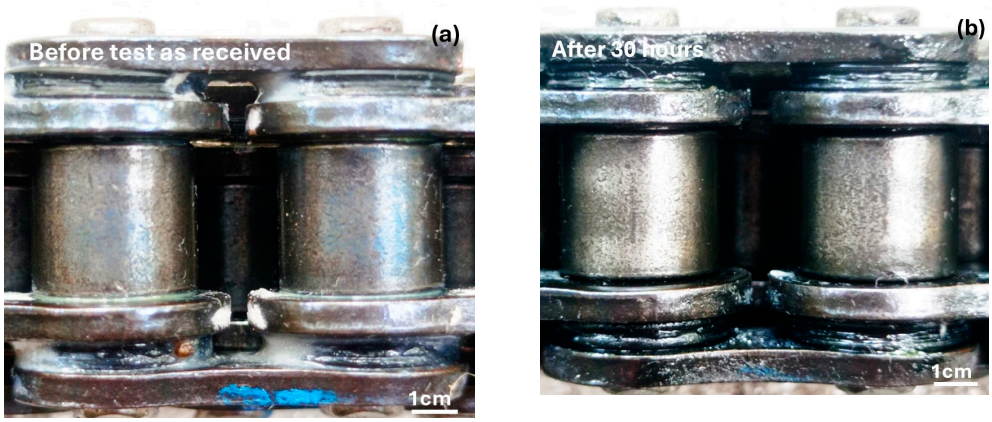


Figure 15. *Cont.*



Figure 15. *Cont.*

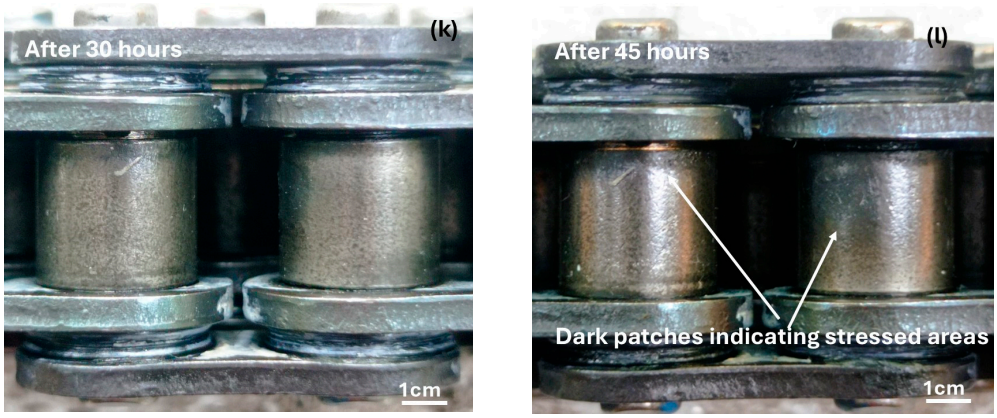


Figure 15. Rollers in (**a**–**c**) dry condition (**d**–**f**) Grade A (**g**–**i**) Grade B (**j**–**l**) Grade C.

4. Conclusions

This work utilizes Industrial Internet of Things components within the tribometer ecosystem. Sensors collect data from the tribo-process and monitor it remotely through the cloud. The work focused on correlating sound and vibrations caused by friction with the coefficient of friction between pins from transmission chains. These tests utilized a reciprocating tribometer and commercial transmission aerosols (Grades A, B, and C). The following conclusions were drawn:

a. Under dry conditions, the CoF (0.5615 ± 0.037) was 41% higher compared to Grade A (0.0335 ± 0.0063) and Grade C (0.0355 ± 0.002), and 28% higher compared to Grade B (0.040 ± 0.0028).

b. All aerosol grades showed similar CoF values. The average WSD was greatest with Grade C (0.401 ± 0.129 mm), followed by Grade A (0.209 ± 0.159 mm) and Grade B (0.204 ± 0.165 mm).

c. Under dry conditions, sound emissions were approximately 60% higher compared to both Grade A and Grade B, and 41% higher than sound levels with Grade C.

d. Vibration levels in the dry condition (0.32 ± 0.127 V) exceeded those of Grade A (0.255 ± 0.007 V) and Grade C (0.260 ± 0.028 V) by around 12%. In contrast, Grade B (0.125 ± 0.007 V) produced vibrations that were 61% lower than those in the dry case and 51% lower than those in Grades A and C.

e. Microscopic examination revealed extensive wear and pronounced tracks under dry conditions. Among the aerosols, Grade A and Grade C showed more surface degradation than Grade B. This matched their higher vibration responses.

f. Surface roughness increased most in dry conditions. Grade A followed by a 6.75% increase, Grade C by 5.32%, and Grade B by 3.21%. The higher roughness for Grades A and C suggests more frequent rupture of the lubricant film and greater metal-to-metal contact.

g. Raman spectroscopy of wear scars detected iron oxide formation. These oxides acted as protective sacrificial layers, reducing direct asperity contact. However, the fragmentation of these oxides contributed to higher acoustic emissions, providing a direct link to the increased sound levels observed during testing. This corroborates the earlier findings regarding sound variations and emphasizes the role of oxide fragmentation in influencing acoustic outcomes.

h. Component-level chain testing demonstrated the superior performance of Grade B, which exhibited lower elongation compared with the other aerosols and dry conditions.

i. Visual inspection of chain rollers confirmed that Grade B lubrication produced fewer stressed regions compared to Grades A and C.

j. ANOVA results showed significant variation across test conditions. Eta-squared values were 95.6% for CoF, 87.1% for WSD, 74.8% for sound, and 70.1% for vibration.

CoF and WSD had statistically significant differences. Changes in sound and vibration were noticeable but not statistically significant. Post hoc analysis showed that all aerosols significantly decreased CoF and WSD compared to dry conditions. Differences among aerosol grades were not statistically significant.

This work showed that measuring sound and vibration during friction can effectively detect chain deterioration. Measuring sound in hard-to-reach places, like covered chain boxes, helps analyze friction. However, analyzing both vibration and sound together allows for more precise conclusions about the equipment's health. A major limitation of sound measurement is surrounding noise. It is highly recommended to consider such noise when investigating the frictional trends of mechanical elements.

5. Future Research Planned

The present work suggests that incorporating elements of the Industrial Internet of Things into mechanical systems facilitates the prediction and analysis of mechanical failures. The current study relies on experimental analysis. Future work will focus on multiscale numerical methods. These methods will couple tribological behavior with acoustic emissions, vibration dynamics, and thermal responses. Models will be integrated with machine learning algorithms and digital twin frameworks. This integration will enable real-time condition monitoring, fault diagnosis, and prediction in diverse environments. To make the models more robust for life cycle predictions, probability approaches and uncertainty quantification will be introduced. Such advanced approaches will enhance the scientific understanding of the interdependencies between friction, wear, and vibration. They will also deliver transformative, smart, autonomous, and self-adaptive mechanical systems.

From the above work, it can be seen that the Industrial Internet of Things is an important concept that needs to be incorporated into mechanical systems, particularly in condition monitoring systems. The data in the cloud, which is collected, stored, and further used for analysis, can be accessed remotely and would be highly beneficial for the predictive maintenance of heavy engineering components.

Author Contributions: Conceptualization, S.B. and K.V.; methodology, S.B., K.V., V.P. and V.F.; software, S.B., K.V. and V.P.; validation, S.B., K.V. and V.P.; formal analysis, S.B., V.P. and V.F.; investigation, S.B., K.V., S.M. (Suruthi Meenachinathan), V.P. and V.F.; resources, S.B., K.V., S.M. (Shail Mavani), V.P. and V.F.; data curation, S.B., K.V., S.V. and S.M. (Suruthi Meenachinathan); writing—original draft preparation, S.B., K.V., S.V. and S.M. (Suruthi Meenachinathan); writing—review and editing, S.M. (Suruthi Meenachinathan), V.P. and V.F.; visualization, S.B., K.V., V.P. and V.F.; supervision, S.B., K.V. and S.M. (Shail Mavani); project administration, S.B. and K.V.; funding acquisition, V.P. and V.F. All authors have read and agreed to the published version of the manuscript.

Funding: This research received no external funding.

Institutional Review Board Statement: Not applicable.

Informed Consent Statement: Not applicable.

Data Availability Statement: Data can be made available from the corresponding author upon reasonable request.

Acknowledgments: The authors acknowledge the support received from M/s Mosil Lubricants P Ltd., Mumbai, for utilizing the test facilities.

Conflicts of Interest: Author Shail Mavani was employed by the Mosil Lubricants Private Limited. The remaining authors declare that the research was conducted in the absence of any commercial or financial relationships that could be construed as a potential conflict of interest.

References

1. Liskiewicz, T. Advancing Surface Engineering for Tribology: From Functionality to Connectivity. *Adv. Eng. Mater.* **2024**, *26*, 2400303. [CrossRef]
2. Atzori, L.; Iera, A.; Morabito, G. The Internet of Things: A survey. *Comput. Netw.* **2010**, *54*, 2787–2805. [CrossRef]
3. Krishnamoorthy, V.; Anitha John, A.; Bhaumik, S.; Paleu, V. Mapping Acoustic Frictional Properties of Self-Lubricating Epoxy-Coated Bearing Steel with Acoustic Emissions during Friction Test. *Technologies* **2024**, *12*, 30. [CrossRef]
4. Matsuoka, K.; Taniguchi, K.; Nakakita, M. In-situ wear monitoring of slider and disk using acoustic emission. *J. Tribol.* **2001**, *123*, 175. [CrossRef]
5. Kita, T.; Kogure, K.; Mitsuya, Y.; Nakanishi, T. New method of detecting contact between floating-head and disk. *IEEE Trans. Magn.* **1980**, *16*, 873–875. [CrossRef]
6. Wada, M.; Mizuno, M. Study on friction and wear utilizing acoustic emission. *J. Jpn. Soc. Precis. Eng.* **1989**, *55*, 673–678. [CrossRef]
7. Taura, H.; Nakayama, K. Behavior of acoustic emissions at the onset of sliding friction. *Tribol. Int.* **2018**, *123*, 155–160. [CrossRef]
8. Ferrer, C.; Salas, F.; Pascual, M.; Orozco, J. Discrete acoustic emission waves during stick–slip friction between steel samples. *Tribol. Int.* **2010**, *43*, 1–6. [CrossRef]
9. Chen, F.; Ouyang, H.; Wang, X. A new mechanism for friction-induced vibration and noise. *Friction* **2023**, *11*, 302–315. [CrossRef]
10. Xu, C.; Li, B.; Wu, T. Wear characterization under sliding–rolling contact using friction-induced vibration features. *Proc. Inst. Mech. Eng. Part J J. Eng. Tribol.* **2021**, *236*, 634–647. [CrossRef]
11. Zhang, L.; Yuan, C.; Dong, C.; Wu, Y.; Bai, X. Friction-induced vibration and noise behaviors of a composite material modified by graphene nano-sheets. *Wear* **2021**, *476*, 203719. [CrossRef]
12. Abdallah, O.; Sassi, S. Contribution of friction-induced vibration to the realistic failure analysis of spur gear cracked teeth. *Eng. Fail. Anal.* **2024**, *158*, 107956. [CrossRef]
13. Qin, H.; Chang, Y.; Zhu, H.; Li, X.; Li, Z.; Xiang, X. Experimental analysis on friction-induced vibration of water-lubricated bearings in a submarine propulsion system. *Ocean Eng.* **2020**, *203*, 107239. [CrossRef]
14. Xue, Y.; Shi, X.; Zhou, H.; Lu, G.; Zhang, J. Effects of groove-textured surface combined with Sn–Ag–Cu lubricant on friction-induced vibration and noise of GCr15 bearing steel. *Tribol. Int.* **2020**, *148*, 106316. [CrossRef]
15. Wang, Y.; Zhang, Y.; Long, R. Influence of Pits on the Tribological Properties and Friction-Induced Vibration Noise of Textured Tapered Roller Bearings. *Tribol. Trans.* **2023**, *66*, 399–412. [CrossRef]
16. Bhaumik, S.; Yunus, M.; Jothikumar, S.; Hareesh, G.; Paleu, V.; Sharma, A.K.; Mavani, S. Exploring the Failures of Deep Groove Ball Bearings Under Alternating Electric Current in the Presence of Commercial Lithium Grease. *Technologies* **2025**, *13*, 275. [CrossRef]
17. Qian, H.; Mo, J.; Xiang, Z.; Fan, Z.; Wu, Y.; Zhou, Z. The effect of the macroscopic surface morphology caused by the uneven wear on friction induced vibration. *Tribol. Int.* **2021**, *154*, 106672. [CrossRef]
18. Chatzi, A.; Doody, O. The one-way ANOVA test explained. *Nurse Res.* **2023**, *31*, 8–14. [CrossRef]
19. Steffy, M.; Bhaumik, S.; Paleu, V. Exploring biotite—A naturally occurring silicate as a sustainable additive in calcium hydroxide/castor oil eco-friendly grease for controlling friction, wear, and energy consumption. *Proc. Inst. Mech. Eng. Part J J. Eng. Tribol.* **2025**. [CrossRef]
20. John, M.M.; Hanief, M.; Khan, M.J. An approach to correlate friction-induced noise with coefficient of friction. *Tribol. Int.* **2025**, *201*, 110253. [CrossRef]
21. James, D.R.; Carpenter, S.H. Relationship between acoustic emissions and dislocations kinetics in crystalline solids. *J. Appl. Phys.* **1971**, *42*, 4685. [CrossRef]
22. Geng, Z.; Puhan, D.; Reddyhoff, T. Using acoustic emission to characterize friction and wear in dry sliding steel contacts. *Tribol. Int.* **2019**, *134*, 394–407. [CrossRef]
23. De Faria, D.L.A.; Venâncio Silva, S.; de Oliveira, M.T. Raman microspectroscopy of some iron oxides and oxyhydroxides. *J. Raman Spectrosc.* **1997**, *28*, 873–878. [CrossRef]

Disclaimer/Publisher's Note: The statements, opinions and data contained in all publications are solely those of the individual author(s) and contributor(s) and not of MDPI and/or the editor(s). MDPI and/or the editor(s) disclaim responsibility for any injury to people or property resulting from any ideas, methods, instructions or products referred to in the content.